ELSEVIER

Contents lists available at ScienceDirect

Computers in Biology and Medicine

journal homepage: www.elsevier.com/locate/compbiomed





Investigation of electro-vascular phase-amplitude coupling during an auditory task

J. McLinden ^a, N. Rahimi ^b, C. Kumar ^b, D.J. Krusienski ^c, M. Shao ^b, K.M. Spencer ^d, Y. Shahriari ^a, ^{*}

- ^a Department of Electrical, Computer, and Biomedical Engineering, University of Rhode Island, Kingston, RI, USA
- ^b Department of Computer and Information Science, University of Massachusetts Dartmouth, MA, USA
- ^c Department of Biomedical Engineering, Virginia Commonwealth University, Richmond, VA, USA
- ^d Department of Psychiatry, VA Boston Healthcare System and Harvard Medical School, Boston, MA, USA

ARTICLE INFO

Keywords:

Electroencephalography (EEG)
Functional near-infrared spectroscopy (fNIRS)
Electro-vascular coupling
Auditory processing
Multimodal neuroimaging

ABSTRACT

Multimodal neuroimaging using electroencephalography (EEG) and functional near-infrared spectroscopy (fNIRS) provides complementary views of cortical processes, including those related to auditory processing. However, current multimodal approaches often overlook potential insights that can be gained from nonlinear interactions between electrical and hemodynamic signals. Here, we explore electro-vascular phase-amplitude coupling (PAC) between low-frequency hemodynamic and high-frequency electrical oscillations during an auditory task. We further apply a temporally embedded canonical correlation analysis (tCCA)-general linear model (GLM)-based correction approach to reduce the possible effect of systemic physiology on fNIRS recordings. Before correction, we observed significant PAC between fNIRS and broadband EEG in the frontal region $(p \ll 0.05)$, β $(p \ll 0.05)$ and γ (p = 0.010) in the left temporal/temporal (left auditory; LA) region, and γ (p = 0.032) in the right temporal/temporoparietal (right auditory; RA) region across the entire dataset. Significant differences in PAC across conditions (task versus silence) were observed in LA (p = 0.023) and RA (p = 0.023) 0.049) γ sub-bands and in lower frequency (5–20 Hz) frontal activity (p = 0.005). After correction, significant fNIRS- γ -band PAC was observed in the frontal (p = 0.021) and LA (p = 0.025) regions, while fNIRS- α (p = 0.003) and fNIRS- β (p = 0.041) PAC were observed in RA. Decreased frontal γ -band (p = 0.008) and increased β -band (p = 0.008) « 0.05) PAC were observed during the task. These outcomes represent the first characterization of electrovascular PAC between fNIRS and EEG signals during an auditory task, providing insights into electro-vascular coupling in auditory processing.

1. Introduction

As noninvasive hybrid brain-computer interface (BCI) studies grow in prominence and approach more widespread adoption, understanding the dynamics between direct and indirect noninvasive neuroimaging modalities becomes more urgent. By simultaneously measuring concurrent neuronal activity and corresponding metabolic changes, it is possible to establish the relationships between the two dynamics and achieve a more comprehensive characterization of neural activity [1]. An improved understanding of neurovascular coupling could elucidate the mechanisms underpinning brain disorders including schizophrenia [2], Parkinson's disease [3], Alzheimer's disease [4–6], among other disorders. Furthermore, characterizing normal electro-vascular

dynamics and identifying changes associated with disease could inform emerging treatment approaches, such as transcranial direct-current stimulation (tDCS), especially in diseases where current pharmacological interventions have demonstrated limited efficacy [7]. As the most common noninvasive technologies used in hybrid BCIs, electroencephalography (EEG) and functional near-infrared technology (fNIRS) have received particular attention in studying the relationships between electrical signals produced by the cerebral cortex and the metabolic signals associated with them [8], which has been bolstered by their portable, complementary, and compatible nature [9]. The complementary information provided by hybrid EEG/fNIRS recording paradigms has been used to more completely characterize functional cortical networks [10] and improve both closed-loop and open-loop BCI

E-mail address: yalda shahriari@uri.edu (Y. Shahriari).

^{*} Corresponding author.

performance [11].

Noninvasive imaging of the neural correlates of auditory processing holds particular value in understanding the processes involved in normal [12,13] and disordered auditory system function, including the disruptions observed in schizophrenia [14], autism spectrum disorder [15], and tinnitus [16]. Developing this understanding can provide treatment targets and inform new treatment approaches, such as neuromodulation via transcranial magnetic stimulation (TMS) [17] or transcranial direct current stimulation (tDCS) [18,19], while also providing information useful for the development of auditory BCIs [20-22]. The study of auditory processing further benefits from noninvasive multimodal signal acquisition approaches. For example, in a recent study, Muñoz-Caracuel et al. (2021) characterized changes in neural responses associated with increasing auditory stimulus intensity, demonstrating simultaneous increasing magnitude of event-related potential (ERP) components and hemodynamic responses [23]. Similarly, Rossi et al. (2011) observed simultaneous increases in EEG N400 responses and greater left hemisphere lateralized hemodynamic responses measured using fNIRS [24]. Steinmetzger et al. (2022) observed right-lateralized differences in EEG ERP responses and hemodynamic activity measured using fNIRS in response to vowel pitch changes [25]. By recording simultaneous EEG and fNIRS, Steinmetzger et al. (2020) were able to propose explanations for unexpected responses in the oxygenated hemoglobin concentration change (ΔHbO₂) time series by comparing with both the deoxygenated hemoglobin concentration change (ΔHbR) time series and with EEG-ERP and frequency domain features [26], demonstrating the advantages of multimodal signal recording in auditory studies.

Although the benefits of simultaneous EEG and fNIRS data acquisition in auditory studies have been demonstrated [23-26], there has been insufficient exploration of the dynamics between the two modalities in this context. One potential challenge in these approaches is related to the nature of hemodynamic signals recorded using fNIRS. Long-separation fNIRS signals, which are typically captured source-detector pairs separated by approximately 3 cm [27], contain cerebral and extracerebral (i.e., scalp) hemodynamic components [28]. By contrast, short-separation fNIRS channels use a shorter (~8 mm) source-detector distance to independently measure scalp hemodynamics for the purpose of further accounting for or removing their influence from the long-separation channels [29]. Physiological sources such as respiration [30] and Mayer waves [31] and non-physiological sources such as movement [32] also contribute to the recorded signal, complicating the estimation of hemodynamic responses. In particular, respiration has been shown to couple with both fNIRS signals [30] and high-frequency EEG oscillations [33-35]. Many of these potential confounding signals have been demonstrated to vary with experimental conditions [36,37]. As fNIRS recordings are affected by multiple potentially unwanted sources of variance (i.e. global hemodynamics, respiration-related oscillations, Mayer waves, etc.), several methods have been proposed to correct for this variance [38-40]. Recent developments in signal analysis approaches including independent measurements (e.g. short-separation fNIRS channels, respiration measurements) of these nuisance signals allow experimenters to account for their contribution to the fNIRS signals recorded using long-separation channels [28]. These developments will allow researchers to further explore the deeply interconnected relationships between electrocortical signals measured using EEG and cortical hemodynamics measured using fNIRS by providing methods to account for the contribution of potential physiological and non-physiological confounds that make exploring these relationships challenging. Such confounds have been shown in previous studies such as Tort et al. (2018), which describes coupling between nasal respiration and several higher frequency oscillations in both cortical and non-cortical brain structures of rats [33].

Despite the challenges in exploring the coupling between electrical oscillations measured by EEG and oscillations in hemodynamic signals

measured by fNIRS, some studies have demonstrated relationships between these oscillations. For example, Pfurtscheller et al. (2012) found a statistically significant correlation between the β-band power envelope in the motor cortex and prefrontal ΔHbO_2 using a bootstrapped crosscorrelation approach [41]. Additionally, Dutta et al. (2015) assessed neurovascular coupling using the cross-correlation between the intrinsic mode functions of both EEG and fNIRS signals generated by empirical mode decomposition [42]. Keles et al. (2016) determined significant cross-correlation between EEG alpha and beta band activity and HbO2 in the parietal and occipital regions [43]. Assessments of neurovascular coupling have also shown group level differences between groups with neurodegenerative disorders and control groups. For example, Chiarelli et al. (2021) reported significantly lower neurovascular coupling in participants with Alzheimer's disease than in a control group. In this study, neurovascular coupling was assessed with a general linear model (GLM)-based approach using features generated by convolving principal components of EEG power time courses with a canonical hemodynamic response function and short-separation fNIRS channels as regressors and long-separation fNIRS channels as the response variable [5]. Many of the reported methods of assessing neurovascular coupling rely on parametric statistical methods, which rely on assumptions about the underlying distribution of the data that may not be met, emphasizing the need for reliable, interpretable non-parametric measures of neurovascular coupling [44]. Additionally, current research exploring electro-vascular coupling has widely relied on the extraction of individual features of each modality and their linear interaction across modalities [44], despite evidence that these interactions may be nonlinear and spatiotemporally nonspecific [45].

In this study, we propose a novel nonlinear approach to investigate electro-vascular phase-amplitude coupling (PAC). We adapt the widely adopted modulation index (MI) approach [46] to quantify the relationship between hemodynamic signals measured using fNIRS and electrical signals obtained using EEG. This investigation was conducted using signals recorded during a block-design auditory task while employing state-of-the-art preprocessing techniques to model and correct for the influence of systemic physiology. To explore the potential sources of observed electro-vascular PAC, we use a GLM-based approach to isolate fNIRS signal components that can be explained by independent measurements of systemic physiology. The objectives of this study are (1) to establish the presence of PAC between the phase of lower frequency hemodynamic signal oscillations during an auditory task in healthy individuals and (2) to explore the possible sources of the observed coupling using a GLM- and temporally embedded canonical correlation (tCCA)-based approach to isolate signal components that can be explained by independent measurements of systemic physiology (i.e., short-separation channels, respiration effort). This novel investigation of interactions between hemodynamic signals and electrocortical oscillations during an auditory task would provide new insights into the metabolic and electrical interactions involved in auditory processing and inform future multimodal neuroimaging studies by exploring instantaneous nonlinear relationships between EEG and fNIRS signals.

2. Methods

2.1. Participants and experimental design

11 participants (age 22.55 ± 3.91 , five female) with no known history of neurological or auditory processing disorder were recruited from the University of Rhode Island (URI). All research activities were approved by the URI institutional review board, and participants provided informed consent prior to participation in the study. Participants completed three runs of an auditory task. Each run consisted of 24 blocks of six 40 Hz white noise click trains of 500 ms duration and 2s interstimulus interval per block presented binaurally through a pair of headphones (Sony Group Corporation). Each stimulus presentation block was followed by a 15s block of silence. A diagram of the

experimental protocol is presented in Fig. 1.

A 15 EEG electrode (256 Hz sampling rate, g.tec g.USBamp, g.tec medical engineering GmbH) and 14 channel fNIRS (7.8125 Hz sampling rate, NIRScout, NIRx medical technologies) montage was used to record neural data. EEG electrodes were placed at locations Fpz, AFz, F5, F6, FCz, FC3, FC4, Cz, C5, C6, TTP7h, TTP8h, TPP7h, TPP8h, and Pz. Eight short-separation fNIRS channels were also recorded, with short-separation detectors embedded in the source housing pads placed at an 8 mm distance from each fNIRS source optode. The experimental montage across modalities is presented in Fig. 2 fNIRS channel locations were selected using the fOLD toolbox to cover the frontal, left auditory, and right auditory regions of interest (ROIs) [47]. These locations were selected due to their relevance to the auditory task employed [14,48]. Respiration signals were recorded alongside EEG signals using a respiration effort belt (256 Hz sampling rate, g.tec medical engineering GmbH).

2.2. Data preprocessing

EEG signal processing was completed using EEGLAB [49] and custom MATLAB scripts. EEG signals from the three collected runs were mean-centered, concatenated, and band-pass filtered 0.5–55 Hz. The first and last 20 s of data corresponding with a pre- and post-run duration were removed from the signal following concatenation and filtering to exclude these data from further analysis. Independent component analysis (ICA) was applied to the EEG data in EEGLAB [49]. Components containing artifacts (eye blinks, motion, instrumentation noise) were visually identified and removed. Raw intensity time series signals collected using fNIRS were converted to ΔHbO_2 time series using the modified Beer-Lambert law and low-pass filtered at 0.5 Hz ΔHbO_2 time series signals were visually inspected and artifactual segments (motion) were marked for later rejection.

2.3. Temporally embedded canonical correlation analysis (tCCA)

In this study, we adopted the temporally embedded canonical correlation analysis (tCCA) approach proposed by von Lühmann et al. (2020) as a comprehensive method for generating nuisance regressors using auxiliary signals recorded from multiple types of sources [50]. This method provides the advantage of accounting for non-instantaneous coupling between measurements of systemic physiology with long-separation channels. In this study, we included the recorded short-separation channels incorporated after visual inspection for data quality and respiration effort signals. These nuisance regressors were then included in the design matrix of a general linear model (GLM) used to model the influence of these regressors on the set of long-separation channels. A modified version of canonical correlation analysis (CCA), a multivariate statistical method that has been commonly applied in physiological signal processing, was used in this

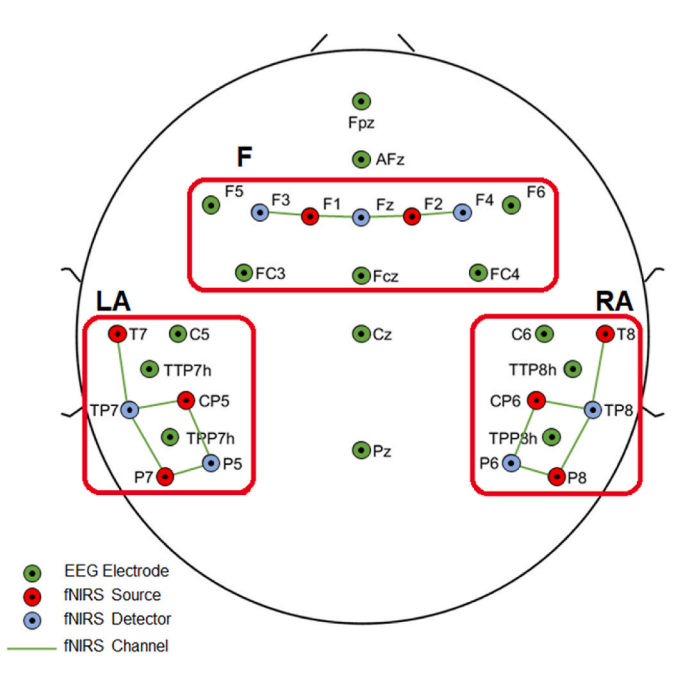


Fig. 2. Experimental montage employed in this study. EEG electrodes are displayed with green dots. fNIRS sources are displayed with red dots, and fNIRS detectors are displayed with blue dots. fNIRS channels are displayed with green lines between source-detector pairs. Short separation detectors were placed a set distance from each source location. Regions of interest (ROIs) are boxed in red

study to find maximally correlated canonical variables representing the two original variable sets of the long-separation channels Y and independent measurements of systemic physiology (short-separation channels and respiration) Z. CCA finds a set of extraction filters w_y, w_z for signals y(t) and z(t) that maximizes the correlation between the two projected signals (i.e. canonical variables):

$$Corr\left(y(t)w_{y},z(t)w_{z}\right) \tag{1}$$

The CCA objective function can also be expressed in block matrix form as a generalized eigenvalue equation:

$$\begin{bmatrix} 0 & C_{yz} \\ C_{zy} & 0 \end{bmatrix} \begin{bmatrix} w_y \\ w_z \end{bmatrix} = \lambda \begin{bmatrix} C_{yy} & 0 \\ 0 & C_{zz} \end{bmatrix} \begin{bmatrix} w_y \\ w_z \end{bmatrix}$$
 (2)

where λ is an eigenvalue, C_{yy} and C_{zz} are the autocovariance matrices of y(t) and z(t), respectively, and C_{yz} and C_{zy} are their cross-covariance matrices. In order to solve this equation, the autocovariance matrices must be invertible, and as such should be regularized as described in Refs. [51,52]. One challenge in the integration of auxiliary signals in

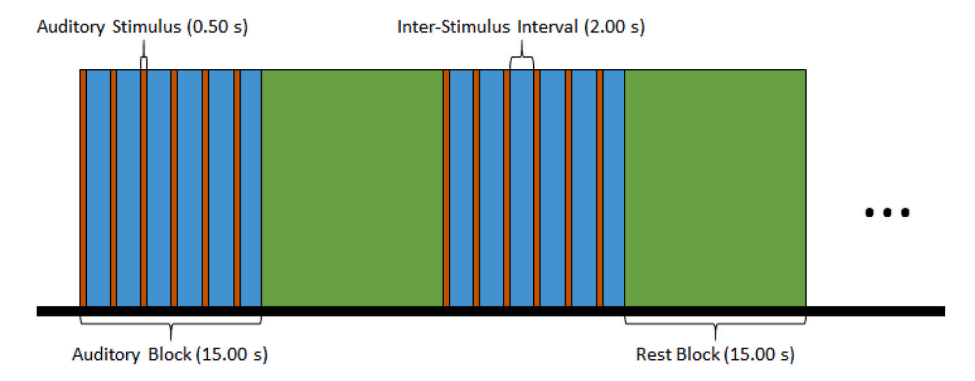


Fig. 1. Experimental task design. Auditory blocks are 15s in duration and consist of the presentation of six 40 Hz white noise click trains of 500 ms duration with a 2s ISI. Rest blocks are 15s in duration.

fNIRS processing pipelines is the non-instantaneous coupling between the auxiliary signals and long-distance data channels, which is assumed by standard CCA. tCCA addresses this problem by finding the ideal time lag τ in the set $\{\tau_0, ..., \tau_D\}$ where D is the number of time lags used to maximize the correlation between the two sets of canonical variables:

$$Corr\left(\sum_{i=0}^{D} y(t)w_{y}, z(t-\tau)w_{z}(\tau_{i})\right)$$
(3)

Hyperparameters include the maximum time lag τ_D , the time step length between time lags Δt , and the correlation threshold ρ set as an inclusion criterion for the GLM design matrix. Canonical variables extracted from the nuisance signals that correlate with the corresponding canonical variables extracted from the fNIRS signals above the correlation threshold are retained, indicated by j, while the remaining are rejected. The j retained tCCA regressors are collected as part of the construction of a design matrix for use in the subsequent GLM analysis.

In this study, parameters used for the tCCA algorithm were selected to fall within the recommended ranges described in von Lühmann et al. (2020) [50]. Specifically, we selected the embedding step width $\Delta t = 0.13$ s (1 sample), maximum absolute time lag $\tau_D = 3.02$ s, and correlation threshold $\rho_{thresh} = 0.4$.

We then constructed a GLM using these regressors and a set of regressors used to represent task information formulated as below:

$$Y = G\beta + E \tag{4}$$

where Y is the matrix of long-separation fNIRS signals, G is the design matrix, β is the set of coefficients, and E is the residual term. G contains a set of regressors used to model the recorded signals, which can include task-related regressors and regressors representing systemic physiology and other nuisance regressors.

In this study, G was generated by appending the tCCA regressors with regressors generated by convolving 15s duration boxcar functions representing the task and the rest blocks with a canonical hemodynamic response (spm, MNE-NIRS toolbox) [53], resulting in j+2 regressors used in the design matrix. A GLM was then fit to the long-separation channel fNIRS data using the constructed design matrix. The coefficients corresponding with the task and the tCCA regressors were separated as below:

$$Y = G_{Task}\beta_{Task} + G_{Phys}\beta_{Phys} + E \tag{5}$$

where G_{Task} and β_{Task} are the collected regressors and weights corresponding with the task, respectively, and G_{Phys} and β_{Phys} are the collected regressors and weights corresponding with the tCCA regressors. The resulting coefficients corresponding to the tCCA regressors were collected and multiplied by their respective columns of the design matrix and subtracted from the original ΔHbO_2 signal to remove all physiological signal components (presumed to be global systemic activity) explained by the GLM to produce $Y_{Corrected}$, which was used in the analysis pipeline along with the original signal Y for comparison as below:

$$Y_{Corrected} = Y - G_{Phys} \beta_{Phys} \tag{6}$$

The fNIRS signals were then upsampled to match the sampling rate of the EEG signals (256 Hz) and runs were concatenated for the subsequent PAC analysis. Adjusted R² and root mean square error (RMSE) were used to quantify model performance [54,55]. Spearman correlation between the number of short channels included and adjusted R² was performed to investigate a possible relationship between the two variables.

2.4. Phase-amplitude coupling (PAC)

We propose electro-vascular phase-amplitude coupling (PAC) as an integrated, nonlinear method to explore interactions between the slow hemodynamic oscillatory activity measured by fNIRS and the fast elec-

trocortical oscillations recorded by EEG. We adapted the algorithm proposed in Tort et al. (2010) [46] for the PAC analysis. To compute PAC between two time series signals x(t) and y(t), the signals were narrow-band filtered into frequency bands of interest $x_{filt}(t)$ and $y_{filt}(t)$ (5 Hz bins in 5 Hz steps from 5-10 Hz to 50–55 Hz for EEG; 0.06–0.5 Hz for fNIRS). Assuming that coupling between the amplitude of x(t) and phase of y(t) is of interest (i.e., x(t) is a preprocessed EEG channel and y(t) is a preprocessed fNIRS channel, either before or after applying the tCCA-GLM preprocessing approach), the Hilbert transform of both signals was taken, and the amplitude envelope of $x_{filt}(t)$ and instantaneous phase of $y_{filt}(t)$ were extracted, denoted $A_x(t)$ and $\varphi_y(t)$, respectively.

The original signals x(t) and y(t) and $A_x(t)$ were visually inspected for artifacts. Marked segments of $A_x(t)$ and $\varphi_y(t)$ were removed from further analysis. These segments included standard 18s windows around each point where the segments were appended to ensure that segments containing discontinuities were not included in the subsequent PAC analysis. This rejection approach was applied as the following steps in the analysis pipeline rely solely on the distributions of data points matched by sample index. Furthermore, in order to confirm the presence of an auditory steady state response (ASSR) in response to the auditory stimuli employed in this study, the power amplitude time series $A_x(t)$ was epoched -0.5:1.0s relative to each auditory stimulus onset averaged across trials, and baseline corrected to the pre-stimulus period.

After the previous steps to ensure signal quality, the phases were binned in N phase bins and the mean value of $A_x(t)$ that corresponded with phase values from $\varphi_y(t)$ in each bin was extracted as $\langle A_x \rangle_\varphi(j)$ for phase bin j. The mean amplitude for each bin was then normalized by the sum over all bins to produce a distribution of mean amplitudes (P) across phase bins as below:

$$P(j) = \frac{\langle A_x \rangle_{\varphi}(j)}{\sum\limits_{k=1}^{N} \langle A_x \rangle_{\varphi}(k)}$$
(7)

A modulation index (MI) value is then extracted as a measure of PAC by normalizing the Kullback-Leibler distance (D_{KL}) between distribution P and the uniform distribution U by log(N) as below:

$$D_{KL}(P, U) = log(N) + \sum_{j=1}^{N} P(j)log[P(j)]$$
(8)

$$MI = \frac{D_{KL}(P, U)}{log(N)} \tag{9}$$

MI is a positive value in [0,1] that increases with increasing PAC between x(t) and y(t). In order to determine whether MI is statistically larger than the value expected by chance with the given data, a surrogate distribution of MI values was then generated. In this study, we followed the method described in Cohen (2014) [56], in which a random time point in the middle 80 % of $A_x(t)$ was selected and the samples were circularly shifted around this point (i.e. appending the end of the later segment to the beginning of the earlier segment). MI was calculated again using this surrogate version of x(t) and this process was repeated M = 200 times to generate a surrogate MI distribution. A p-value corresponding with each MI value was determined by taking the ratio of the number of surrogate MI values greater than the observed MI value to M. This surrogate distribution was then used to convert the observed MI value to a z-score as below:

$$MI_{z} = \frac{MI_{Observed} - mean(MI_{Distribution})}{std(MI_{Distribution})}$$
(10)

A permutation clustering-based approach applied across participants was used to identify statistically significant spatio-spectral clusters of PAC. By conducting a one-sample t-test across participants for MI_z corresponding to each frequency band/channel combination across modalities, test statistics (t-statistics) were generated to compare with the t-

statistics obtained from another surrogate distribution. The surrogate *t*statistics were obtained by performing a one-sample t-test on permutations generated by changing the sign of the observed test statistics (2047 permutations, corresponding with the total number of possible permutations across 11 participants). A p-value for each EEG/fNIRS channel pair and EEG/fNIRS frequency band was then generated by taking the ratio of the number of surrogate t-values greater than the observed tvalue to the number of permutations. After this, p-values below a predefined threshold (p < 0.05) were clustered based on spectro-spatial adjacency and the sum of the test statistics within each are calculated. Spectral adjacency was defined as adjacent EEG frequency bands, while EEG and fNIRS sensors from the same ROI were considered spatially adjacent. A cluster p-value was then calculated for each cluster by taking the ratio of the number of surrogate test statistic sums from the largest cluster greater than the observed cluster test statistic sum to the number of permutations. This permutation clustering approach provides a framework for a non-parametric statistical test to find spectro-spatial clusters of PAC across a participant population that is robust to the multiple comparisons problem [57]. Similarly, this permutation clustering approach can be used to compare PAC across conditions. In this case, PAC calculated within each condition was compared across participants using a paired sample t-test. The surrogate distribution was similarly constructed by changing the labels of each of the PAC values observed across participants and recomputing the test statistic.

3. Results

3.1. Electro-vascular PAC

Fig. 3 illustrates the general analysis pipeline employed in this study. EEG and fNIRS signals were preprocessed as previously described and statistical PAC between the two signals was extracted.

Fig. 4 displays significant cluster t-statistics obtained from our analysis before and after applying tCCA regressor removal. Our outcomes demonstrated four significant PAC clusters before applying tCCA-GLM regressor removal. The first cluster (cluster $t=24.76,\,p=4.885e-04$) includes broadband EEG in the 15–55 Hz range in the frontal (F) region. Two significant clusters are observed in the left auditory (LA) region, with one appearing in the 15–25 Hz range (cluster $t=18.60,\,p=4.885e-04$), and the second appearing in the 30–50 Hz range (cluster $t=18.60,\,p=4.885e-04$).

15.74, p=0.010). A fourth cluster appears from 35 to 50 Hz in the right auditory (RA) region (cluster t = 13.75, p=0.032). After tCCA regressor removal, we observe one cluster in the F region in the 30–50 Hz range (cluster t = 15.24, p=0.021). Another significant cluster (cluster t = 10.79, p=0.025) appears in the LA region in the 40–50 Hz range. Two clusters appear in the RA region, with one appearing in the 10–20 Hz range (cluster t = 16.47, p=0.003) and another in the 25–35 Hz range (cluster t = 9.30, p=0.041).

3.2. Comparisons across conditions (task and rest)

Fig. 5 displays cluster t-values from significant positive (top row) and negative (bottom row) clusters across the task and rest conditions before (left column) and after (right column) applying tCCA regressor removal. Comparing across conditions, two positive clusters (i.e., stronger PAC in the task condition than in the rest condition) were observed before tCCA regressor removal (Fig. 5 top left). We observed a positive cluster in the 30–45 Hz range (cluster t = 16.26, p = 0.023) in the LA region, while another positive cluster in the 45–55 Hz range (cluster t = 13.69, p =0.049) was observed in the RA region. We also observed a significant negative cluster (i.e., stronger PAC in the rest condition than in the task condition) in the 5-20 Hz range before tCCA regressor removal (cluster t = -19.90, p = 0.0049) (Fig. 5 bottom left). After tCCA regressor removal, one significant positive cluster (cluster t = 14.93, p = 0.00) was observed in the 20-35 Hz range in the F region, while one significant negative cluster (cluster t = -12.70, p = 0.0083) was observed in the same region (Fig. 5 top and bottom right).

3.3. tCCA regressor removal

Table 1 displays the average adjusted R^2 of the GLM across all long-separation channels for each participant after applying the tCCA-GLM pipeline to model the influence of respiration effort and short-separation channels along with the number of short detectors (NumSDs) included in the tCCA feature generation algorithm. On average, the adjusted R^2 value was 0.73 \pm 0.14, corresponding with an approximate 73 % of variance in the long-separation channels explained by modeling using the short-separation and respiration effort channels and an average of 5.73 \pm 2.00 short channels were eventually retained per participant. The average RMSE across channels and participants was

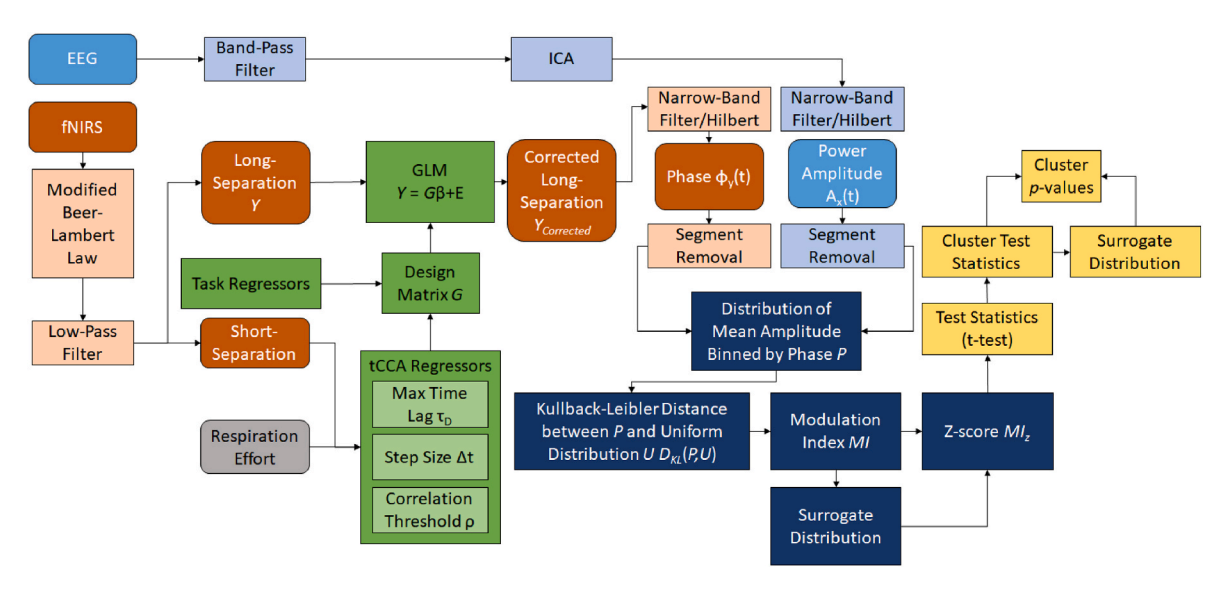


Fig. 3. Block diagram of the proposed analysis pipeline. EEG signals were preprocessed using a band-pass filtering/ICA approach. fNIRS signals were low-pass filtered and converted to the oxygenated hemoglobin change time series (ΔHbO_2) using the modified beer-lambert law. The tCCA-GLM correction approach is applied to long-separation channels, and the resulting EEG and fNIRS signals are further narrow-band filtered and the Hilbert transform of both signals is taken. Instantaneous EEG power amplitude and fNIRS phase are fed to the phase-amplitude coupling algorithm, and significant clusters of coupling are identified using the proposed permutation clustering approach.

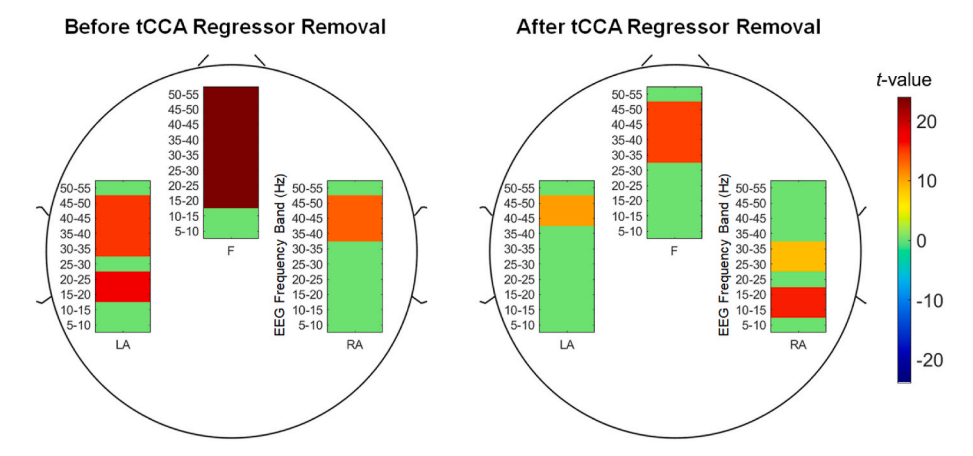


Fig. 4. Cluster t-statistics corresponding to significant clusters within each ROI before (left) and after (right) tCCA regressor removal.

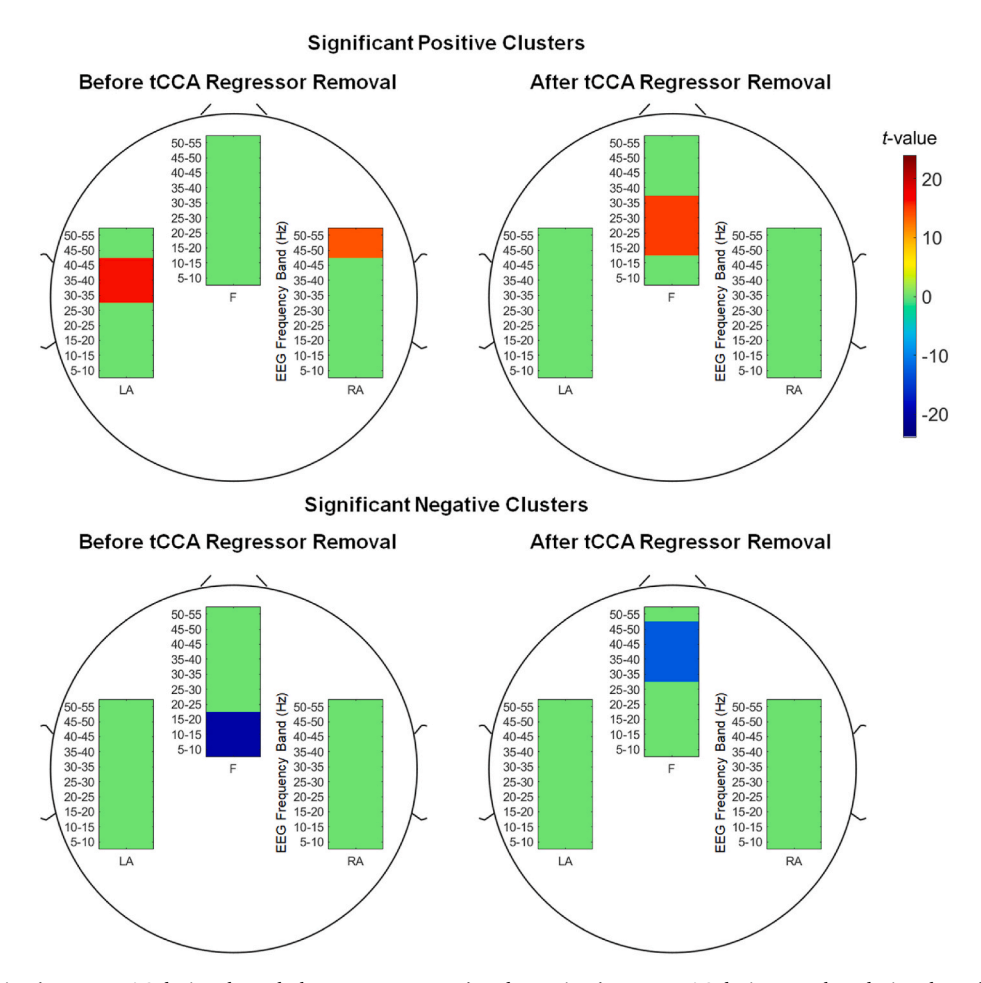


Fig. 5. Significant positive (stronger PAC during the task than at rest; top row) and negative (stronger PAC during rest than during the task; bottom row) cluster t-value maps that correspond with PAC clusters across conditions before (left column) and after (right column) tCCA regressor removal.

 $20.42\pm7.72~\mu M.$ Spearman correlation between adjusted R^2 and the number of short detectors included determined a significant relationship between the two (Spearman $\rho=0.77, p=0.005$). Fig. 6 illustrates the original, modeled, and difference between the original and modeled ΔHbO_2 time courses from a representative participant/channel (S01, F3–F1). Fig. 7 (A) depicts the average response from the same representative participant/channel across experimental blocks.

3.4. EEG-auditory steady-state response (ASSR)

The grand average of baseline corrected power amplitude across participants at channel FCz is presented in Fig. 7 (B). A clear ASSR is visible in the 35–45 Hz range, while auditory ERP components are reflected in the 5–15 Hz range.

4. Discussion

This study investigated the interactions between slow hemodynamic

Table 1Average adjusted R² and RMSE across channels of the GLM used in the tCCA-GLM filtering approach for each participant, along with the number of short detectors (NumSDs) included in the tCCA feature generation algorithm.

Participant	Adjusted R ²	RMSE (μM)	NumSDs
S01	0.86	20.32	8
S02	0.84	17.19	7
S03	0.88	10.70	7
S04	0.58	38.00	2
S05	0.68	23.61	7
S06	0.53	17.16	4
S07	0.87	15.56	6
S08	0.56	28.42	3
S09	0.88	16.94	8
S10	0.75	13.23	5
S11	0.65	23.50	6
Average	0.73 ± 0.14	20.42 ± 7.72	5.73 ± 2.00

oscillations measured using fNIRS and fast electrocortical oscillations recorded using EEG during an auditory task. The results of this study mark the initial documented instance of characterizing electro-vascular phase-amplitude coupling (PAC) between fNIRS and EEG. Within the scope of this investigation, we have successfully identified, for the first time, statistically significant clusters that demonstrate the existence of electro-vascular PAC. This coupling was observed between the instantaneous phase of slow hemodynamics fNIRS signals and instantaneous

power amplitude of high frequency EEG signals during an auditory task. We assessed these interactions before and after applying a tCCA-GLM-based fNIRS correction strategy to the recorded long-separation fNIRS signals to determine the effect of global hemodynamic activity on this relationship. We further explored differences in observed PAC across task conditions to investigate the role of electro-vascular PAC in auditory processing.

Our analysis demonstrated that the adopted correction strategy could model a substantial (~73 % \pm 14 %) proportion of the variance of long-separation channels averaged over channels and participants. Our correlation analysis suggested a relationship between adjusted $\rm R^2$ and the number of short-separation channels available. This finding agrees with previous literature, including a study conducted by Santosa et al. (2020) demonstrating an increase in the percentage of short-channel variance explained with an increase in the number of short channels with diminishing returns as more short channels are included [58]. Given the substantial percentage of variance in the long-separation channels that can be modeled using the short-separation channels and respiration effort, the long-separation channels before applying the correction strategy may reflect more global changes in the participants' hemodynamic state, while long-separation channels after the correction may reflect more localized cerebral hemodynamics.

Our outcomes further demonstrated significant (p < 0.05) coupling across the entire dataset in different frequency bands in all three regions of interest (ROIs) both before and after applying the proposed correction strategy. The presence of these clusters of PAC between fNIRS and EEG

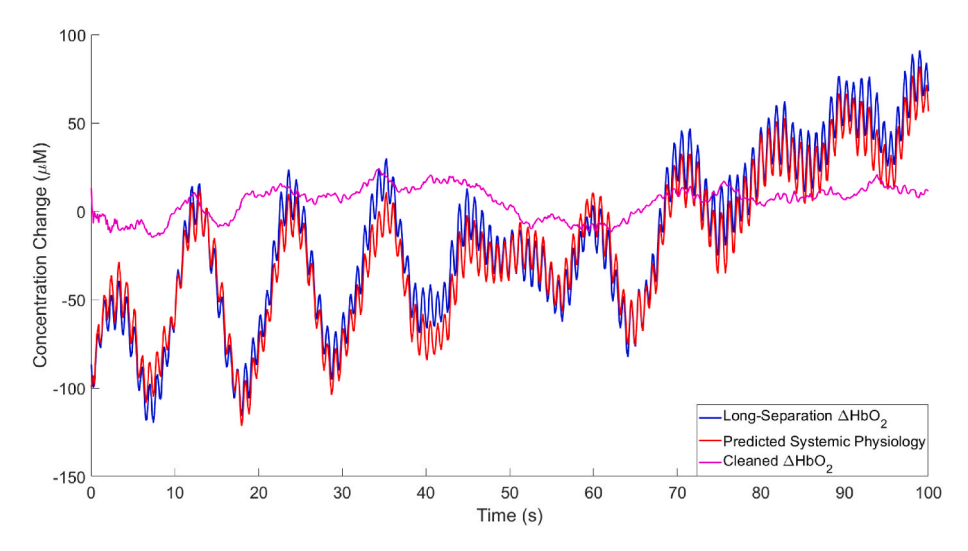


Fig. 6. Observed (blue) and modeled (red) ΔHbO_2 time courses from a representative participant using the tCCA-GLM based approach. The cleaned ΔHbO_2 signal (magenta) is the difference between the observed and modeled ΔHbO_2 signals.

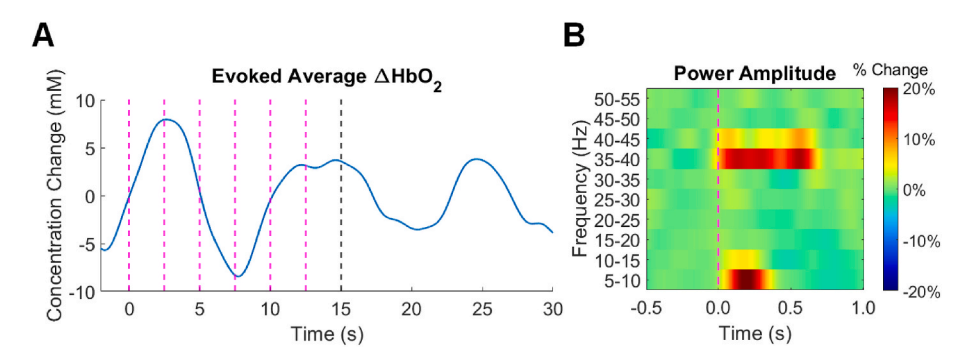


Fig. 7. A) Evoked average Δ HbO2 signal from a representative participant/channel (S01, F3–F1). The vertical dashed magenta lines denote auditory stimulus onset, while the vertical black dashed line represents the onset of the rest period. B) Percentage change of the grand average power amplitude from representative channel FCz relative to the -0.5:0.0s pre-stimulus period. Auditory stimulus onset is denoted by a magenta vertical dashed line. A clear ASSR is visible in the 35–45 Hz bands, while ERP components are reflected in the 5–15 Hz band.

across the three ROIs could be attributed to several possible sources. One possibility is that PAC between respiration and EEG could be reflected in these results. Respiration has been identified as a source of interference in fNIRS signals [59], and we and other groups have demonstrated to couple with multiple frequency bands across several cortical regions [35,60,61] including the frontal and left/right temporal/temporoparietal regions. Respiration-γ-band coupling is one of the more commonly reported instances of this phenomenon and is thought to reflect a modulatory effect of respiration on cortical excitability [35]. The presence of broad coupling in the frontal region and γ -band coupling in the left auditory and right auditory regions before correction could potentially be explained by respiration signal components in fNIRS signals. It is plausible that other sources of systemic physiology reflected in fNIRS could play a role in the differences in PAC observed before and after correction. For example, heart rate variability (HRV), which can also be reflected in fNIRS signals, has been demonstrated to modulate spectral features in EEG in the α , β , and γ bands [62]. However, the presence of significant PAC clusters in each region after correction suggests that other electro-vascular interactions may take place. This finding provides further evidence for nonlinear interactions between cerebral hemodynamics and electrical oscillatory activity, which could have possible implications for future hybrid EEG-fNIRS BCI studies. Currently, these studies predominantly consider linear unimodal methods for feature extraction [9]. Although the proposed PAC approach requires a prohibitive amount of data to be used as a feature in a single-trial BCI application, our findings suggest instantaneous coupling between EEG and fNIRS signals that could be informative in future studies.

When comparing across conditions, the presence of significant positive and negative PAC clusters suggests that electro-vascular coupling is present and related to multiple sources of activity involved in the different conditions. General brain-body interactions have been reported [63], but remain underexplored to date. Notably, Zelano et al. (2016) observed PAC between nasal respiration and electrocortical activity, and that this relationship could have a role in influencing cognitive processing [61]. Another example is the presence of PAC between parietal/occipital alpha and the phase of the gastric basal rhythm reported by Richter et al. (2017) [64]. PAC has also been demonstrated within fNIRS channels, with lower frequency signal components reflecting neurogenic activity and higher frequency signal components reflecting systemic physiology (respiration and cardiac components) [65]. The results observed before correction suggest that our observed electro-vascular coupling could be related to several processes associated with the task. The positive left auditory cluster suggests increased gamma coupling with long-separation fNIRS channels during the task when compared with rest. As this cluster was not present after correction, it is possible that this could reflect coupling between global hemodynamic components (cardiac, Mayer waves, respiration, etc.) and ASSR amplitude. The observed positive right auditory gamma cluster extends to the limits of the bands explored in this analysis, which were selected due to the 1/f fall-off of relative power observed in scalp EEG measurements [66]. It is possible that this cluster could extend further into higher EEG frequency bands, but the nonspecificity in the EEG frequency domain compared to the observed left auditory cluster and lateral position could possibly reflect electromyographic (EMG) activity [67]. The significant negative cluster in the frontal region overlapped with the frequency bands reflecting ERP components during the task. Although no coupling was observed in this region before or after applying the correction strategy across the entire dataset, it is possible that the presence of ERPs that do not change in amplitude relative to the phase values of the hemodynamic signal could reduce coupling relative to that observed during resting periods.

Our outcomes demonstrated significant electro-vascular PAC clusters in the frontal and left auditory regions between fNIRS and EEG in different γ sub-bands after applying the correction strategy. We observed that both sub-bands (frontal, 30–50 Hz and left auditory, 40–50 Hz) overlapped with auditory stimulation frequency, which may

suggest that evoked power attributed to the ASSR may be modulated by the phase of hemodynamic signals. The frontal/frontocentral region is notable for being the location typically reported in ASSR studies, as this response is typically maximal in the frontal region [68]. Interestingly, the observed PAC coupling was found to be stronger in this band in the frontal region during the rest condition than during the task condition. This could possibly reflect electro-vascular decoupling in this band during the task as a result of the ASSR associated with this frequency band. Electro-vascular coupling at rest could be disrupted by the presence of the ASSR in this band, which would be larger in amplitude when compared to resting state γ -band activity.

The left auditory region may be of interest as well, as the left auditory cortex has demonstrated a role in the processing of the rapid temporal characteristics of sound, as opposed to the right auditory cortex's role in the processing of pitch [69]. Our analysis showed no significant difference across conditions in this band/region. Additionally, the two lower frequency clusters appearing in the right auditory region after the correction strategy lack a clear explanation in the context of the task. Right-lateralized α-band activity is associated with auditory anticipation [70], and could be a factor in the repetitive task employed for this study. Similarly, β-band oscillations have also been implicated in auditory prediction [71]. It is possible that the phase of cortical hemodynamics could be related to anticipation of stimuli via PAC. There was no significant difference across conditions in bands containing either of these clusters, however, suggesting that this coupling may occur independent of the task. The significant positive cluster observed after correction in the β band could possibly reflect hemodynamic modulation of attention-related processes, as frontal β band activity has been related to attention [72].

The outcomes from this study have demonstrated significant clusters of coupling between low-frequency hemodynamic signals, measured using fNIRS, and high-frequency electrical oscillations, measured by EEG, during auditory settings. We assessed this coupling both prior to and following the implementation of a tCCA-GLM-based correction strategy to limit any potential influence of systemic physiology that might have led to any observed coupling, expanding on previous characterizations of electro-vascular coupling in which this consideration was not made [41,73] or nonlinear spectro-temporal features of fNIRS signals were not considered [5]. To the best of our knowledge, this study represents the first attempt to characterize any potential interactions between hemodynamic and electrocortical oscillations during auditory tasks. Furthermore, our results suggest that this electro-vascular PAC may be both task-dependent and task-independent, and that the instantaneous hemodynamic state could possibly influence multiple cortical processes simultaneously.

The interpretations of the current findings are limited by the sample size of this study, which limits the statistical power of the current analyses. Although comparisons were made across experimental conditions, the number of samples available in each condition provides relatively few (~60) cycles of the lowest frequency of interest (0.06 Hz) in the within-condition analysis [46]. Furthermore, the limited number of sensor locations for each modality restricts the comprehensive characterization of coupling. We additionally only consider one fNIRS frequency band due to the exploratory nature of this study; consideration of separate distinct fNIRS sub-bands could provide further information. Finally, the current electro-vascular coupling exclusively examines instantaneous coupling between the two modalities. However, it remains plausible that a more comprehensive characterization of these relationships could be achieved by adopting an approach that accounts for variable delays in coupling, such as the convolution of spectral power curves with a pre-defined hemodynamic response function [74]. Future work should be conducted to optimize this approach with respect to temporal variability in this relationship by adopting optimization methods, such as evolutionary algorithms [75,76]. However, this study characterizes task-independent and task dependent electro-vascular PAC, providing a framework for further investigation of cross-modal

nonlinear measurements of electro-vascular coupling, while providing evidence for its involvement in auditory task-related and task-independent processes.

CRediT authorship contribution statement

J. McLinden: Conceptualization, Data curation, Formal analysis, Investigation, Methodology, Software, Validation, Visualization, Writing – original draft, Writing – review & editing. N. Rahimi: Methodology, Writing – original draft. C. Kumar: Methodology, Writing – original draft. D.J. Krusienski: Conceptualization, Validation, Writing – original draft. M. Shao: Funding acquisition, Methodology, Writing – original draft. K.M. Spencer: Conceptualization, Funding acquisition, Investigation, Methodology, Validation, Visualization, Writing – original draft. Y. Shahriari: Conceptualization, Funding acquisition, Investigation, Methodology, Project administration, Resources, Software, Supervision, Validation, Visualization, Writing – original draft, Writing – review & editing.

Declaration of competing interest

None Declared.

Acknowledgments

This work was supported by the National Science Foundation [NSF-2024418]. The authors would like to thank the participants who took part in this study, without whom this study would not have been possible.

References

- [1] H. Obrig, et al., Habituation of the visually evoked potential and its vascular response: implications for neurovascular coupling in the healthy adult, Neuroimage 17 (1) (Sep. 2002) 1–18, https://doi.org/10.1006/nimg.2002.1177.
- [2] S. Schneider, L. Wagels, F.B. Haeussinger, A.J. Fallgatter, A.-C. Ehlis, A.M. Rapp, Haemodynamic and electrophysiological markers of pragmatic language comprehension in schizophrenia, World J. Biol. Psychiatr. 16 (6) (Sep. 2015) 398–410, https://doi.org/10.3109/15622975.2015.1019359.
- [3] M. Abtahi, et al., Merging fNIRS-EEG brain monitoring and body motion capture to distinguish Parkinsons disease, IEEE Trans. Neural Syst. Rehabil. Eng. 28 (6) (Jun. 2020) 1246–1253, https://doi.org/10.1109/TNSRE.2020.2987888.
- [4] D. Perpetuini, et al., Working memory decline in Alzheimer's disease is detected by complexity analysis of multimodal EEG-fNIRS, Entropy 22 (12) (Dec. 2020), https://doi.org/10.3390/e22121380.
- [5] A.M. Chiarelli, et al., Evidence of neurovascular un-coupling in mild Alzheimer's disease through multimodal EEG-fNIRS and multivariate analysis of resting-state data, Biomedicines 9 (4) (Mar. 2021), https://doi.org/10.3390/ biomedicines9040337
- [6] R. Li, T. Nguyen, T. Potter, Y. Zhang, Dynamic cortical connectivity alterations associated with Alzheimer's disease: an EEG and fNIRS integration study, Neuroimage Clin 21 (2019), 101622, https://doi.org/10.1016/j.nicl.2018.101622.
- [7] D. Yang, Y.-I. Shin, K.-S. Hong, Systemic review on transcranial electrical stimulation parameters and EEG/fNIRS features for brain diseases, Front. Neurosci. 15 (2021), 629323, https://doi.org/10.3389/fnins.2021.629323.
- [8] R. Li, D. Yang, F. Fang, K.-S. Hong, A.L. Reiss, Y. Zhang, Concurrent fNIRS and EEG for brain function investigation: a systematic, methodology-focused review, Sensors 22 (15) (Aug. 2022), https://doi.org/10.3390/s22155865.
- [9] K.-S. Hong, M.J. Khan, M.J. Hong, Feature extraction and classification methods for hybrid fNIRS-EEG brain-computer interfaces, Front. Hum. Neurosci. 12 (2018) 246, https://doi.org/10.3389/fnhum.2018.00246.
- [10] W.-C. Su, et al., Simultaneous multimodal fNIRS-EEG recordings reveal new insights in neural activity during motor execution, observation, and imagery, Sci. Rep. 13 (1) (Mar. 2023) 5151, https://doi.org/10.1038/s41598-023-31609-5.
- [11] S.B. Borgheai, et al., Enhancing communication for people in late-stage ALS using an fNIRS-based BCI system, IEEE Trans. Neural Syst. Rehabil. Eng. 28 (5) (May 2020) 1198–1207, https://doi.org/10.1109/TNSRE.2020.2980772.
- [12] E. Demeter, B. Glassberg, M.L. Gamble, M.G. Woldorff, Reward magnitude enhances early attentional processing of auditory stimuli, Cognit. Affect Behav. Neurosci. 22 (2) (Apr. 2022) 268–280, https://doi.org/10.3758/s13415-021-00962-1.
- [13] X. Guo, P. Dheerendra, E. Benzaquén, W. Sedley, T.D. Griffiths, EEG Responses to auditory figure-ground perception, Hear. Res. 422 (Sep. 2022), 108524, https:// doi.org/10.1016/j.heares.2022.108524.

- [14] Y. Hirano, N. Oribe, S. Kanba, T. Onitsuka, P.G. Nestor, K.M. Spencer, Spontaneous gamma activity in schizophrenia, JAMA Psychiatr. 72 (8) (Aug. 2015) 813–821, https://doi.org/10.1001/jamapsychiatry.2014.2642.
- [15] C. Vlaskamp, et al., Auditory processing in autism spectrum disorder: mismatch negativity deficits, Autism Res. 10 (11) (Nov. 2017) 1857–1865, https://doi.org/ 10.1002/aur.1821.
- [16] J. Zhang, et al., Switching Tinnitus-On: maps and source localization of spontaneous EEG, Clin. Neurophysiol. 132 (2) (Feb. 2021) 345–357, https://doi. org/10.1016/i.clinph.2020.10.023.
- [17] R. Lorentzen, T.D. Nguyen, A. McGirr, F. Hieronymus, S.D. Østergaard, The efficacy of transcranial magnetic stimulation (TMS) for negative symptoms in schizophrenia: a systematic review and meta-analysis, Schizophrenia (Heidelb) 8 (1) (Apr. 2022) 35, https://doi.org/10.1038/s41537-022-00248-6.
- [18] W.-L. Jiang, et al., Adjunctive tDCS for treatment-refractory auditory hallucinations in schizophrenia: a meta-analysis of randomized, double-blinded, sham-controlled studies, Asian J Psychiatr 73 (Jul. 2022), 103100, https://doi.org/ 10.1016/j.ajp.2022.103100.
- [19] T. Elyssa Kok, R. Schaette, G.S. Shekhawat, Impact of tDCS and HD-tDCS on tinnitus perception: a scoping review, Prog. Brain Res. 262 (2021) 225–244, https://doi.org/10.1016/bs.pbr.2020.05.002.
- [20] K.-S. Hong, H. Santosa, Decoding four different sound-categories in the auditory cortex using functional near-infrared spectroscopy, Hear. Res. 333 (Mar. 2016) 157–166, https://doi.org/10.1016/j.heares.2016.01.009.
- [21] N. Kaongoen, S. Jo, A novel hybrid auditory BCI paradigm combining ASSR and P300, J. Neurosci. Methods 279 (Mar. 2017) 44–51, https://doi.org/10.1016/j. ineumeth 2017 01 011
- [22] J. Xiao, et al., An auditory BCI system for assisting CRS-R behavioral assessment in patients with disorders of consciousness, Sci. Rep. 6 (Sep. 2016), 32917, https://doi.org/10.1038/srep32917.
- [23] M. Muñoz-Caracuel, V. Muñoz, F.J. Ruíz-Martínez, D. Di Domenico, S. Brigadoi, C. M. Gómez, Multivariate analysis of the systemic response to auditory stimulation: an integrative approach, Exp. Physiol. 106 (4) (Apr. 2021) 1072–1098, https://doi.org/10.1113/EP089125.
- [24] S. Rossi, I.B. Jürgenson, A. Hanulíková, S. Telkemeyer, I. Wartenburger, H. Obrig, Implicit processing of phonotactic cues: evidence from electrophysiological and vascular responses, J. Cognit. Neurosci. 23 (7) (Jul. 2011) 1752–1764, https://doi. org/10.1162/jocn.2010.21547.
- [25] K. Steinmetzger, E. Megbel, Z. Shen, M. Andermann, A. Rupp, Cortical activity evoked by voice pitch changes: a combined fNIRS and EEG study, Hear. Res. 420 (Jul. 2022), 108483, https://doi.org/10.1016/j.heares.2022.108483.
- [26] K. Steinmetzger, Z. Shen, H. Riedel, A. Rupp, Auditory cortex activity measured using functional near-infrared spectroscopy (fNIRS) appears to be susceptible to masking by cortical blood stealing, Hear. Res. 396 (Oct. 2020), 108069, https:// doi.org/10.1016/j.heares.2020.108069.
- [27] M. Ferrari, V. Quaresima, A brief review on the history of human functional near-infrared spectroscopy (fNIRS) development and fields of application, Neuroimage 63 (2) (Nov. 2012) 921–935, https://doi.org/10.1016/j.neuroimage.2012.03.049.
- [28] S. Tak, J.C. Ye, Statistical analysis of fNIRS data: a comprehensive review, Neuroimage 85 (Pt 1) (Jan. 2014) 72–91, https://doi.org/10.1016/j. neuroimage.2013.06.016.
- [29] S. Brigadoi, R.J. Cooper, How short is short? Optimum source-detector distance for short-separation channels in functional near-infrared spectroscopy, Neurophotonics 2 (2) (Apr. 2015), 025005, https://doi.org/10.1117/1. NPh. 2.2.025005.
- [30] A. Aarabi, T.J. Huppert, Characterization of the relative contributions from systemic physiological noise to whole-brain resting-state functional near-infrared spectroscopy data using single-channel independent component analysis, Neurophotonics 3 (2) (Apr. 2016), 025004, https://doi.org/10.1117/1. NPh.3.2.025004.
- [31] M.A. Yücel, et al., Mayer waves reduce the accuracy of estimated hemodynamic response functions in functional near-infrared spectroscopy, Biomed. Opt Express 7 (8) (Aug. 2016) 3078–3088, https://doi.org/10.1364/BOE.7.003078.
- [32] B. Molavi, G.A. Dumont, Wavelet-based motion artifact removal for functional near-infrared spectroscopy, Physiol. Meas. 33 (2) (Feb. 2012) 259–270, https://doi.org/10.1088/0967-3334/33/2/259.
- [33] A.B.L. Tort, J. Brankačk, A. Draguhn, Respiration-entrained brain rhythms are global but often overlooked, Trends Neurosci. 41 (4) (Apr. 2018) 186–197, https://doi.org/10.1016/j.tins.2018.01.007.
- [34] W. Zhong, et al., Selective entrainment of gamma subbands by different slow network oscillations, Proc. Natl. Acad. Sci. U. S. A. 114 (17) (Apr. 2017) 4519–4524, https://doi.org/10.1073/pnas.1617249114.
- [35] J.L. Herrero, S. Khuvis, E. Yeagle, M. Cerf, A.D. Mehta, Breathing above the brain stem: volitional control and attentional modulation in humans, J. Neurophysiol. 119 (1) (Jan. 2018) 145–159, https://doi.org/10.1152/jn.00551.2017.
- [36] J. Zhang, X. Yu, D. Xie, Effects of mental tasks on the cardiorespiratory synchronization, Respir. Physiol. Neurobiol. 170 (1) (Jan. 2010) 91–95, https://doi.org/10.1016/j.resp.2009.11.003.
- [37] A. Rochet-Capellan, S. Fuchs, Changes in breathing while listening to read speech: the effect of reader and speech mode, Front. Psychol. 4 (2013) 906, https://doi. org/10.3389/fpsyg.2013.00906.
- [38] E. Kirilina, et al., The physiological origin of task-evoked systemic artefacts in functional near infrared spectroscopy, Neuroimage 61 (1) (May 2012) 70–81, https://doi.org/10.1016/j.neuroimage.2012.02.074.
- [39] A. von Lühmann, Z. Boukouvalas, K.-R. Müller, T. Adalı, A new blind source separation framework for signal analysis and artifact rejection in functional Near-

- Infrared Spectroscopy, Neuroimage 200 (Oct. 2019) 72–88, https://doi.org/10.1016/j.neuroimage.2019.06.021.
- [40] Xian Zhang, Jack Adam Noah, Joyce Hirsch, Separation of the global and local components in functional near-infrared spectroscopy signals using principal component spatial filtering, Neurophotonics 3 (1) (Feb. 2016) 1–8, https://doi. org/10.1117/1.NPh.3.1.015004.
- [41] G. Pfurtscheller, I. Daly, G. Bauernfeind, G.R. Müller-Putz, Coupling between intrinsic prefrontal HbO2 and central EEG beta power oscillations in the resting brain, PLoS One 7 (8) (2012), e43640, https://doi.org/10.1371/journal. pone.0043640.
- [42] A. Dutta, A. Jacob, S.R. Chowdhury, A. Das, M.A. Nitsche, EEG-NIRS based assessment of neurovascular coupling during anodal transcranial direct current stimulation—a stroke case series, J. Med. Syst. 39 (4) (Apr. 2015) 205, https://doi. org/10.1007/s10916-015-0205-7.
- [43] H.O. Keles, R.L. Barbour, A. Omurtag, Hemodynamic correlates of spontaneous neural activity measured by human whole-head resting state EEG+fNIRS, Neuroimage 138 (Sep. 2016) 76–87, https://doi.org/10.1016/j. neuroimage.2016.05.058.
- [44] M.K. Yeung, V.W. Chu, Viewing neurovascular coupling through the lens of combined EEG-fNIRS: a systematic review of current methods, Psychophysiology 59 (6) (Jun. 2022), e14054, https://doi.org/10.1111/psyp.14054.
- [45] A.M. Chiarelli, F. Zappasodi, F. Di Pompeo, A. Merla, Simultaneous functional near-infrared spectroscopy and electroencephalography for monitoring of human brain activity and oxygenation: a review, Neurophotonics 4 (4) (Oct. 2017), 041411, https://doi.org/10.1117/1.NPh.4.4.041411.
- [46] A.B.L. Tort, R. Komorowski, H. Eichenbaum, N. Kopell, Measuring phase-amplitude coupling between neuronal oscillations of different frequencies, J. Neurophysiol. 104 (2) (Aug. 2010) 1195–1210, https://doi.org/10.1152/jn.00106.2010.
- [47] G.A. Zimeo Morais, J.B. Balardin, J.R. Sato, fNIRS Optodes' Location Decider (fOLD): a toolbox for probe arrangement guided by brain regions-of-interest, Sci. Rep. 8 (1) (Feb. 2018) 3341, https://doi.org/10.1038/s41598-018-21716-z.
- [48] R.P. Kennan, S.G. Horovitz, A. Maki, Y. Yamashita, H. Koizumi, J.C. Gore, Simultaneous recording of event-related auditory oddball response using transcranial near infrared optical topography and surface EEG, Neuroimage 16 (3 Pt 1) (Jul. 2002) 587–592, https://doi.org/10.1006/nimg.2002.1060.
- [49] A. Delorme, S. Makeig, EEGLAB: an open source toolbox for analysis of single-trial EEG dynamics including independent component analysis, J. Neurosci. Methods 134 (1) (Mar. 2004) 9–21, https://doi.org/10.1016/j.ineumeth.2003.10.009.
- [50] A. von Lühmann, X. Li, K.-R. Müller, D.A. Boas, M.A. Yücel, Improved physiological noise regression in fNIRS: a multimodal extension of the General Linear Model using temporally embedded Canonical Correlation Analysis, Neuroimage 208 (Mar. 2020), 116472, https://doi.org/10.1016/j.neuroimage.2019.116472.
- [51] B. Blankertz, S. Lemm, M. Treder, S. Haufe, K.-R. Müller, Single-trial analysis and classification of ERP components—a tutorial, Neuroimage 56 (2) (May 2011) 814–825, https://doi.org/10.1016/j.neuroimage.2010.06.048.
- [52] O. Ledoit, M. Wolf, A well-conditioned estimator for large-dimensional covariance matrices, J. Multivariate Anal. 88 (2) (2004) 365–411.
- [53] E. Larson, et al., "MNE-Python." Zenodo (Aug. 2023), https://doi.org/10.5281/ zenodo.8262487.
- [54] A. Srivastava, V. Singhal, A. Aggarawal, Comparative analysis of multimodal medical image fusion using PCA and wavelet transforms, International journal of latest technology in engineering, management & applied science 6 (4) (Apr. 2017) 115–118.
- [55] F. Zhang, D. Cheong, A.F. Khan, Y. Chen, L. Ding, H. Yuan, Correcting physiological noise in whole-head functional near-infrared spectroscopy, J. Neurosci. Methods 360 (Aug. 2021), 109262, https://doi.org/10.1016/j. ineumeth.2021.109262.
- [56] M. Cohen, Analyzing Neural Time Series Data, Massachusetts Institute of Technology, Cambridge, Massachusetts, 2014.
- [57] E. Maris, R. Oostenveld, Nonparametric statistical testing of EEG- and MEG-data, J. Neurosci. Methods 164 (1) (Aug. 2007) 177–190, https://doi.org/10.1016/j. ineumeth.2007.03.024.
- [58] H. Santosa, X. Zhai, F. Fishburn, P.J. Sparto, T.J. Huppert, Quantitative comparison of correction techniques for removing systemic physiological signal in functional

- near-infrared spectroscopy studies, Neurophotonics 7 (3) (Jul. 2020), 035009, https://doi.org/10.1117/1.NPh.7.3.035009.
- [59] N. Hakimi, et al., Estimation of respiratory rate from functional near-infrared spectroscopy (fNIRS): a new perspective on respiratory interference, Biosensors 12 (12) (Dec. 2022), https://doi.org/10.3390/bios12121170.
- [60] J. McLinden, et al., Phase-amplitude coupling between EEG cortical oscillations and respiration: an exploratory study, presented at the 11th International IEEE EMBS Conference on Neural Engineering (2023). https://ieeexplore.ieee.org/do cument/10123888
- [61] C. Zelano, et al., Nasal respiration entrains human limbic oscillations and modulates cognitive function, J. Neurosci. 36 (49) (Dec. 2016) 12448–12467, https://doi.org/10.1523/JNEUROSCI.2586-16.2016.
- [62] M. Pardo-Rodriguez, E. Bojorges-Valdez, O. Yanez-Suarez, Bidirectional intrinsic modulation of EEG band power time series and spectral components of heart rate variability, Auton. Neurosci. 232 (May 2021), 102776, https://doi.org/10.1016/j. autneu.2021.102776.
- [63] W. Klimesch, The frequency architecture of brain and brain body oscillations: an analysis, Eur. J. Neurosci. 48 (7) (Oct. 2018) 2431–2453, https://doi.org/10.1111/ ein.14192.
- [64] C.G. Richter, M. Babo-Rebelo, D. Schwartz, C. Tallon-Baudry, Phase-amplitude coupling at the organism level: the amplitude of spontaneous alpha rhythm fluctuations varies with the phase of the infra-slow gastric basal rhythm, Neuroimage 146 (Feb. 2017) 951–958, https://doi.org/10.1016/j. neuroimage.2016.08.043.
- [65] Z. Liu, et al., Monitoring the depth of anesthesia based on phase-amplitude coupling of near-infrared spectroscopy signals, IEEE Trans. Neural Syst. Rehabil. Eng. 31 (2023) 2849–2857, https://doi.org/10.1109/TNSRE.2023.3289183.
- [66] B. Voytek, R.T. Knight, Dynamic network communication as a unifying neural basis for cognition, development, aging, and disease, Biol. Psychiatr. 77 (12) (Jun. 2015) 1089–1097, https://doi.org/10.1016/j.biopsych.2015.04.016.
- [67] I.I. Goncharova, D.J. McFarland, T.M. Vaughan, J.R. Wolpaw, EMG contamination of EEG: spectral and topographical characteristics, Clin. Neurophysiol. 114 (9) (Sep. 2003) 1580–1593, https://doi.org/10.1016/S1388-2457(03)00093-2.
- [68] D. Koshiyama, et al., Source decomposition of the frontocentral auditory steady-state gamma band response in schizophrenia patients and healthy subjects, Psychiatr. Clin. Neurosci. 75 (5) (May 2021) 172–179, https://doi.org/10.1111/pcn.13201.
- [69] R.J. Zatorre, P. Belin, Spectral and temporal processing in human auditory cortex, Cerebr. Cortex 11 (10) (Oct. 2001) 946–953, https://doi.org/10.1093/cercor/ 11.10.946.
- [70] H.A. ElShafei, R. Bouet, O. Bertrand, A. Bidet-Caulet, Two sides of the same coin: distinct sub-bands in the α rhythm reflect facilitation and suppression mechanisms during auditory anticipatory attention, eNeuro 5 (4) (Aug. 2018), https://doi.org/ 10.1523/ENEURO.0141-18.2018.
- [71] D. Meijer, E. Te Woerd, P. Praamstra, Timing of beta oscillatory synchronization and temporal prediction of upcoming stimuli, Neuroimage 138 (Sep. 2016) 233–241, https://doi.org/10.1016/j.neuroimage.2016.05.071.
- [72] A. Angelidis, W. van der Does, L. Schakel, P. Putman, Frontal EEG theta/beta ratio as an electrophysiological marker for attentional control and its test-retest reliability, Biol. Psychol. 121 (Pt A) (Dec. 2016) 49–52, https://doi.org/10.1016/j. bionsycho.2016.09.008.
- [73] P. Lachert, D. Janusek, P. Pulawski, A. Liebert, D. Milej, K.J. Blinowska, Coupling of Oxy- and Deoxyhemoglobin concentrations with EEG rhythms during motor task, Sci. Rep. 7 (1) (Nov. 2017), 15414, https://doi.org/10.1038/s41598-017-15770.2
- [74] R.I. Goldman, J.M. Stern, J.J. Engel, M.S. Cohen, Simultaneous EEG and fMRI of the alpha rhythm, Neuroreport 13 (18) (Dec. 2002) 2487–2492, https://doi.org/ 10.1097/01.wnr 0000047685 08940 d0
- [75] S. Chauhan, M. Singh, A.K. Aggarwal, Investigative analysis of different mutation on diversity-driven multi-parent evolutionary algorithm and its application in area coverage optimization of WSN, Soft Comput. 27 (14) (Jul. 2023) 9565–9591, https://doi.org/10.1007/s00500-023-08090-3.
- [76] S. Chauhan, M. Singh, A.K. Aggarwal, Designing of optimal digital IIR filter in the multi-objective framework using an evolutionary algorithm, Eng. Appl. Artif. Intell. 119 (Mar. 2023), 105803, https://doi.org/10.1016/j. engappai.2022.105803.